JAAS

View Article Online
View Journal | View Issue

Experimental determination of ruthenium L-shell fluorescence yields and Coster–Kronig transition probabilities

Nils Wauschkuhn, [ID] * Katja Frenzel, [ID] Burkhard Beckhoff and Philipp Hönicke [ID]

The L-shell fluorescence yields and the Coster–Kronig factors of ruthenium (and the corresponding uncertainty) were determined for the first time experimentally by applying radiometrically calibrated instrumentation of the Physikalisch-Technische Bundesanstalt. The resulting fluorescence yields ($\omega_{L_3} = 0.0459(20)$, $\omega_{L_2} = 0.0415(26)$, $\omega_{L_1} = 0.0109(9)$) and the Coster–Kronig factors ($f_{23} = 0.177(32)$, $f_{13} = 0.528(90)$, $f_{12} = 0.173(73)$) agree reasonable well with parts of the data from the literature.

1 Introduction

Ruthenium is a versatile and widely used chemical element playing a crucial role in important areas of science and technology. Several applications in the area of semiconductor fabrication or catalysis can be identified, where ruthenium is essential. For extreme ultraviolet lithography masks[1,2] or as interconnect metal[3–5] either ruthenium or ruthenium-containing materials are very relevant. In catalysis, ruthenium-based catalysts provide remarkable properties in several different applications.[6] In addition to this, ruthenium is also of relevance for emerging applications for energy storage[7,8] and medicine.[9,10]

But, if X-ray fluorescence (XRF) based techniques are to be used for determining the ruthenium content in such materials, one quickly finds that the knowledge of the relevant atomic fundamental parameter (FP) data for ruthenium is very limited: for ruthenium, especially its L-shell FP data and namely the L-subshell fluorescence yields and Coster–Kronig factors (CK), no experimentally determined data seems to exist so far. Available data in the literature is either purely theoretically determined or perhaps even less favorable, only interpolated employing adjacent chemical elements. As these FPs quantitatively describe the process of X-ray fluorescence generation, they are very crucial for most quantification approaches in XRF. Thus, they have a direct influence on the accuracy of the XRF quantification results.

As this is a highly inadequate situation, we applied the PTB's reference-free X-ray spectrometry toolset in order to experimentally determine the fluorescence yields and the Coster–Kronig factors of the L-subshells of ruthenium for the first time. Based on transmission and fluorescence experiments on thin

film samples, such FP data can be derived as already demonstrated for a wide range of chemical elements.[11–15]

2 Experimental procedure

For an experimental determination of L-shell fluorescence yields and Coster–Kronig transition probabilities, both fluorescence- and transmission experiments with a selective excitation of the three L-subshells on either a free standing thin foil or a thin coating on a carrier foil are required.[11–13,15] In the present work, these experiments were conducted on the four-crystal monochromator (FCM) beamline[16] of BESSY II using a vacuum chamber that is in-house developed.[17] This chamber was endowed with a silicon drift detector (SDD) of which the detection efficiency is radiometrically calibrated and the response functions are determined experimentally.[18] The employed sample was a highly homogeneous 150 nm ruthenium deposition on a 500 nm Si_3N_4 membrane. To be able to isolate the ruthenium contribution from the total sample transmission, also a blank membrane of nominally identical thickness was used. Any potential moderate variation in the Si_3N_4 membrane thickness is only a second-order contribution to the uncertainties. Both samples were positioned in the chamber's center by using an x–y-scanning stage. The angle between the incoming beam and the sample as well as the angle between sample surface and detector was set to 45°.

The transmission measurements were conducted in an energy range around the Ru-L absorption edges between 2.1 keV and 4 keV. Furthermore, X-ray fluorescence measurements were performed in the incident-energy domain between 2.8 keV and 3.4 keV. The established methodology[11,12,19,20] to derive the relevant L-shell FPs from this experimental dataset is described in the following.

According to the Sherman equation,[21] the measured count rate of fluorescence photons of a one-elemental foil, which is irradiated under 45°, is the product of the fluorescence

Physikalisch-Technische Bundesanstalt, Abbestr. 2-12, 10587 Berlin, Germany. E-mail: nils.wauschkuhn@ptb.de
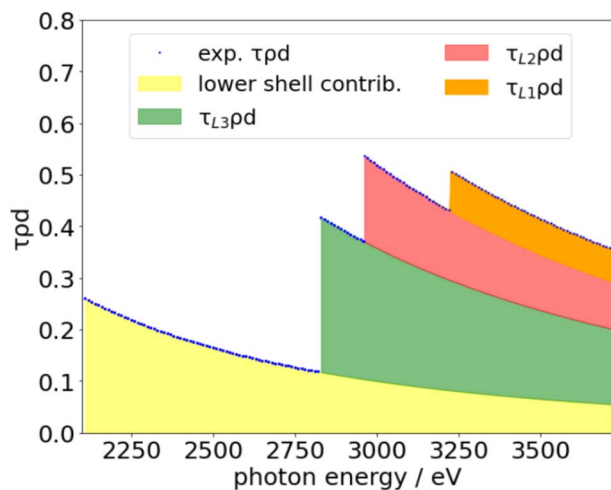
This journal is © The Royal Society of Chemistry 2023

J. Anal. At. Spectrom., 2023, **38**, 1301–1306 | **1301**

Fig. 1 $\tau_S(E_0)\rho d$ determined for the ruthenium thin film: separation of the contributions of lower bound shells (yellow), L_3 (green), L_2 (red) and L_1 (orange).

Table 1 Comparison of the experimentally determined Ru-L-subshell fluorescence yields and Coster–Kronig factors with the X-raylib database[25] [version 4.0.0] and other values (values from compilations (comp.) and theoretic values) from the literature

	Ru ω_{L_3}	Ru ω_{L_2}	Ru ω_{L_1}
This work (XRF)	0.0459(20)	0.0415(26)	0.0109(9)
X-raylib[25] (comp.)	0.043	0.040	0.012
Krause[26] (comp.)	0.043(9)	0.040(10)	0.012(4)
Perkins et al.[29] (comp.)	0.045231	0.043368	0.0084138
McGuire[28] (theory)	0.0450	0.0418	0.00774
Puri et al.[27] (theory)	0.045	0.043	0.0083
Xu et al.[30] (comp.)			0.015

	Ru f_{23}	Ru f_{13}	Ru f_{12}
This work (XRF)	0.177(32)	0.528(90)	0.173(73)
X-raylib[25] (comp.)	0.144	0.61	0.10
Krause[26] (comp.)	0.148(30)	0.61(7)	0.10(2)
McGuire[28] (theory)	0.136	0.779	0.057
Puri et al.[27] (theory)	0.140	0.766	0.057

production cross section σ_{Li} of the considered shell, the incoming $\Phi_0(E_0)$ as well as the fluorescence photon flux $\Phi_i^d(E0)$, the detection efficiency of the SDD, the mass deposition of that element, the attenuation correction factor M_{i,E_0} and the solid angle Ω of detection of the SDD.

The self-attenuation correction factor takes into account the attenuation of the incident radiation and of the fluorescence radiation on its way through the sample. The corresponding sample-specific attenuation correction factor M_{i,E_0} is determined by transmission experiments taking advantage of the fact, that the knowledge of the ruthenium deposition thickness d and its density ρ is not needed since they appear only in a product with the mass absorption coefficient μ_S or with the subshell photoionization cross section τ_S. The product $\mu_S\rho d$ is derived from the transmittance data using the Lambert–Beer law.

For incident energies E_0 between the L_3 edge and the L_2 edge, the fluorescence production factor for the L_3-subshell is

$$\sigma_{L_3}(E_0)\rho d = \omega_{L_3}\tau_{L_3}(E_0)\rho d = \frac{\Phi_i^d(E_0)M_{i,E_0}}{\Phi_0(E_0)\frac{\Omega}{4\pi}}, \tag{1}$$

where ω_{L_3} is the ruthenium L_3 fluorescence yield which should be determined. The sample-specific attenuation correction factor M_{i,E_0} is defined as

$$M_{i,E_0} = \frac{\left(\frac{\mu_S(E_0)\rho d}{\sin\theta_{in}} + \frac{\mu_S(E_i)\rho d}{\sin\theta_{out}}\right)}{\left(1 - \exp\left[-\left(\frac{\mu_S(E_0)\rho d}{\sin\theta_{in}} + \frac{\mu_S(E_i)\rho d}{\sin\theta_{out}}\right)\right]\right)}. \tag{2}$$
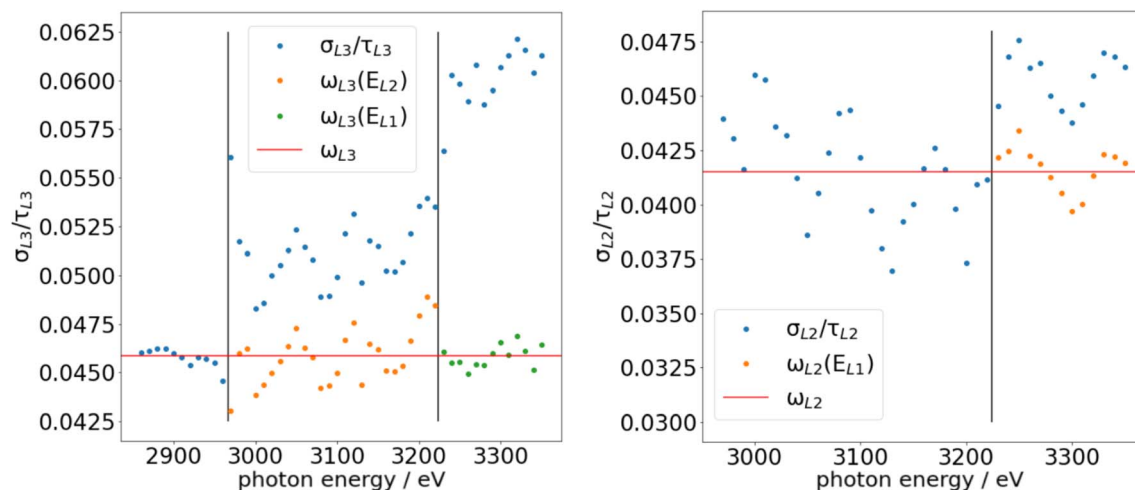

Fig. 2 Experimental determination of the Ru-L_3 (left image) and Ru-L_2 (right image) fluorescence yields: they are determined by averaging over all considered energies where only the respective shell is excited (below L_2 for ω_{L_3} and below L_1 for ω_{L_2}). Using these ω_{L_3} and ω_{L_2}, the Coster–Kronig factors are determined in such a way that the average in the higher energy domains matches the ω_{Li} value.

1302 | J. Anal. At. Spectrom., 2023, 38, 1301–1306

This journal is © The Royal Society of Chemistry 2023

Here, θ_{in} is the angle between the incident beam and the sample surface, θ_{out} is the angle between the sample surface and the SDD detector.

Due to the so-called Coster–Kronig effect, the effective photoionization cross section $\tau_{eff,Li}(E_0)$ for L_3 and L_2 is a linear combination with the higher bound shells since for photon
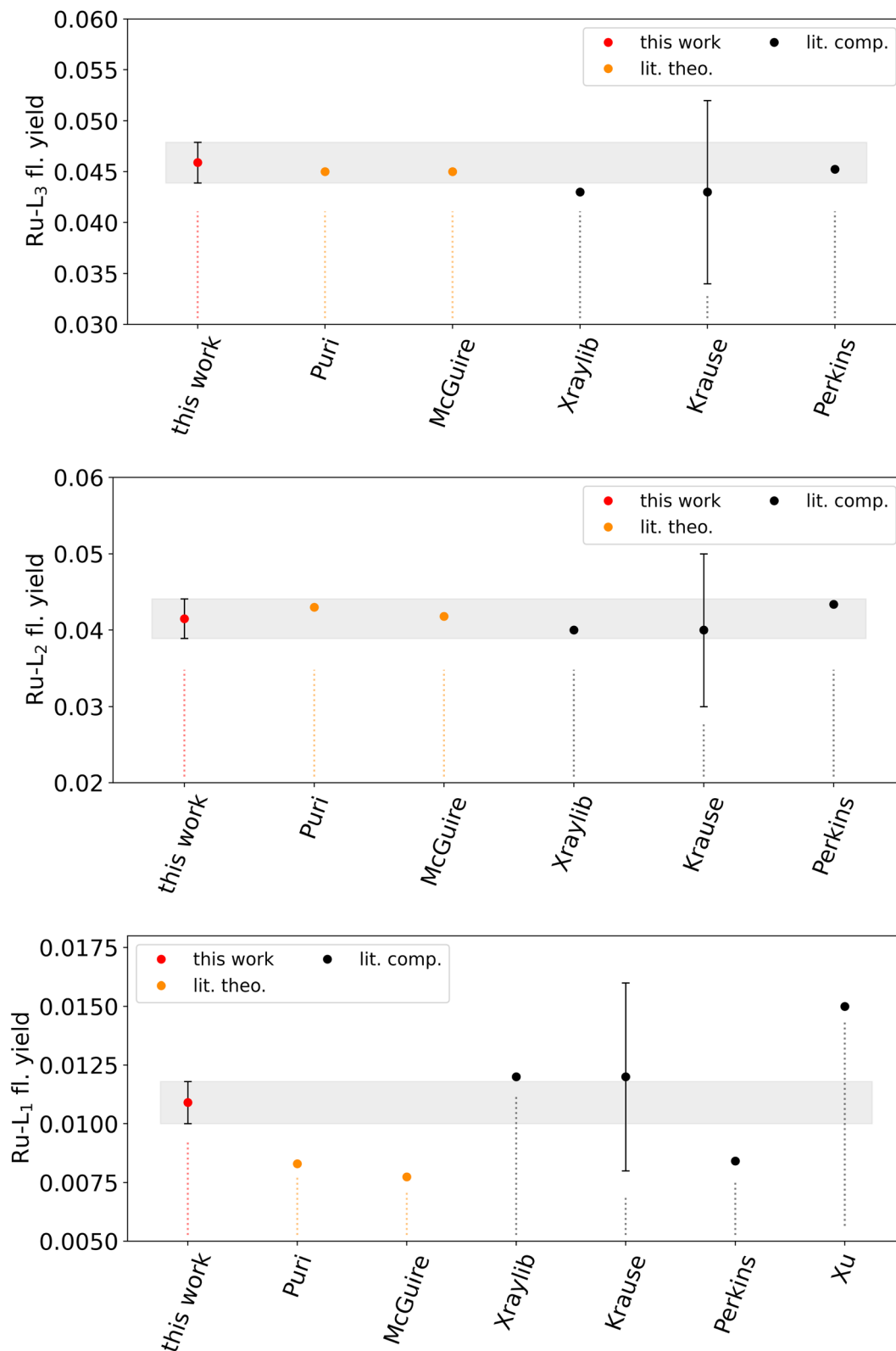

Fig. 3 Comparison of the experimentally determined Ru-L-subshell fluorescence yields with values from the literature.

This journal is © The Royal Society of Chemistry 2023

J. Anal. At. Spectrom., 2023, **38**, 1301–1306 | **1303**

energies above the excitation energy of the next subshell, created holes in L_2 can decay into L_3 by ejecting outer electrons. As a result, more than the directly created holes in L_3 exist. The CK-factor f_{23} provides the probability for this to happen and similar transitions can occur between the L_1 and the L_2 and L_3 shells. So for an incident photon energy above the L_1 threshold, the fluorescence production factors are defined as:

$$\tau_{\text{eff},L_3}(E_0) = \tau_{L_3}(E_0) + f_{23}\tau_{L_2}(E_0) + [f_{13} + f_{12}f_{23}]\tau_{L_1}(E_0) \quad (3)$$

$$\tau_{\text{eff},L_2}(E_0) = \tau_{L_2}(E_0) + f_{12}\tau_{L_1}(E_0) \quad (4)$$

$$\tau_{\text{eff},L_1}(E_0) = \tau_{L_1}(E_0) \quad (5)$$

Here, the $\tau_{Li}(E_0)$ are the photoionization cross sections of the respective L_i subshell,[19] and f_{ij} are the Coster–Kronig factors. For incident energies below the subsequent subshell, the corresponding subshell photoionization cross section is zero ($\tau_{Li}(E_0) = 0$ for $E_0 < E_{Li}$). Therefore, the fluorescence yields are determined for energies E_0 above the excitation energy of the considered and below the subsequent subshell.

All relevant observables are accessible from the experimental data as $\mu_S\rho d$ are determined for the relevant energies by measuring the transmission of the ruthenium coating. $\Phi_i^d(E0)$ is determined by spectral deconvolution of the recorded SDD spectra considering the relevant fluorescence lines and relevant background contributions such as bremsstrahlung. $\Phi_0(E_0)$ and Ω are known because of PTB's calibrated instrumentation.[22]

Taking into account the theoretical ratio of scattering to ionization cross sections, which one can take from databases,[23] the sample-specific total photoionization cross section $\tau_S\rho d$ can be derived. To isolate the subshell contributions of the different τ_{Li}, Ebel polynomials[23] for each L_i contribution as well as a total cross section for lower bound shells are scaled into the data (see Fig. 1). For this scaling process, only the datapoints slightly above each absorption edge are used to minimize the effect of the fine structure.

With these determined $\tau_{Li}\rho d$, the equations for the fluorescence production cross sections can be solved for ω_{Li}. By replacing τ_{Li} by the effective photoionization cross section according to eqn (3)–(5), eqn (1) can be applied also for energies above the next subshell. Therefore, to determine f_{23}, energies between E_{L_3} and E_{L_2} were considered, see Fig. 2: with the already determined ω_{L_3}, the modified version of eqn (1) can be solved for f_{23}. f_{12} is determined in the same way but applied for the fluorescence of the L_2 shell and for $E_{L_2} < E_0 < E_{L_1}$ with the already determined ω_{L_2}. With these determined f_{23} and f_{12}, from the fluorescence of the L_3 shell for energies above E_{L_1}, f_{13} can be determined.

3 Results

The determined fluorescence yields are $\omega_{L_3} = 0.0459(20)$, $\omega_{L_2} = 0.0415(26)$ and $\omega_{L_1} = 0.0109(9)$. The resulting Coster–Kronig factors are $f_{23} = 0.177(32)$, $f_{13} = 0.528(91)$ and $f_{12} = 0.173(73)$. These values are compared with values from the literature in Table 1 and Fig. 3 and 4. The respective uncertainties were
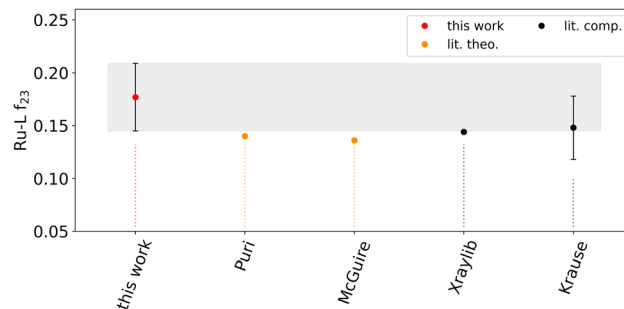

Fig. 4 Comparison of the experimentally determined Coster–Kronig factor f_{23} with values from the literature.

calculated *via* error propagation. The main contributions to the total uncertainty budget of the fluorescence yields were arising from the spectral deconvolution (~2%) and from the photoionization cross sections (~2%). The uncertainty budget is calculated by applying the reference-free XRF approach for the FP determination, discussed in more detail in ref. 24.

The X-raylib[25] and Krause[26] values of ω_{L_3} and ω_{L_1} are slightly outside of the error domain of the values determined in this work. The agreement with respect to the theoretically calculated data of Puri[27] and McGuire[28] is better in the case of ω_{L_3} but even worse for ω_{L_1}. The data of Perkins[29] as well as the data by Xu[30] behaves very similarly. For ω_{L_2}, all available data from the literature agrees well with the result obtained here. With respect to the Coster–Kronig factors, the tabulated data in X-raylib and the Krause compilation is in good agreement with our results. However, the results are on or slightly outside the boundary of our uncertainty budget for all three CK values. The data by McGuire and Puri is outside of our results considering their uncertainty budget.

4 Conclusion

The Coster–Kronig factors and the fluorescence yields of ruthenium are determined experimentally by applying PTB's radiometrically calibrated instrumentation. The values determined are in reasonably good agreement with the values from the literature, although some literature values are slightly outside the uncertainty ranges of this work. The magnitude of the determined uncertainties of this work is much lower than the estimated uncertainties of Krause[26] in the case of the fluorescence yield values. With respect to the Coster–Kronig factors, similar uncertainties were achieved here. In summary, this uncertainty reduction will positively influence the total uncertainties of fundamental parameter-based quantitative X-ray fluorescence experiments.As stated already in previous works of our group,[14,15,24,31] the X-raylib database is also in the case of the Ru-L shell fundamental parameters a reliable reference.

Conflicts of interest

There are no conflicts to declare.

1304 | *J. Anal. At. Spectrom.*, 2023, **38**, 1301–1306

This journal is © The Royal Society of Chemistry 2023

Acknowledgements

References

1 M. Wu, J. F. de Marneffe, K. Opsomer, C. Detavernier, A. Delabie, P. Naujok, et al., Characterization of $Ru_{4-x}Tax$ (x = 1,2,3) alloy as material candidate for EUV low-n mask, Micro Nano Eng., 2021, 12, 100089. Available from: https://www.sciencedirect.com/science/article/pii/S2590007221000101.

2 V. Philipsen, K. V. Luong, K. Opsomer, L. Souriau, J. Rip, C. Detavernier, et al., Mask absorber development to enable next-generation EUVL, in Photomask Japan 2019: XXVI Symposium on Photomask and Next-Generation Lithography Mask Technology, ed. A. Ando, International Society for Optics and Photonics. SPIE, 2019, vol. 11178, p. 111780F, DOI: 10.1117/12.2537967.

3 L. G. Wen, C. Adelmann, O. V. Pedreira, S. Dutta, M. Popovici, B. Briggs, et al., Ruthenium metallization for advanced interconnects, in IEEE International Interconnect Technology Conference/Advanced Metallization Conference, IITC/AMC, 2016, pp. 34–36.

4 K. Barmak, S. Ezzat, R. Gusley, A. Jog, S. Kerdsongpanya, A. Khaniya, et al., Epitaxial metals for interconnects beyond Cu, J. Vac. Sci. Technol. A, 2020, 38(3), 033406, DOI: 10.1116/6.0000018.

5 S. Kondati Natarajan, C. L. Nies and M. Nolan, The role of Ru passivation and doping on the barrier and seed layer properties of Ru-modified TaN for copper interconnects, J. Chem. Phys., 2020, 152(14), 144701, DOI: 10.1063/5.0003852.

6 R. Gramage-Doria and C. Bruneau, Ruthenium-catalyzed C–H bond functionalization in cascade and one-pot transformations, Coord. Chem. Rev., 2021, 428, 213602. https://www.sciencedirect.com/science/article/pii/S0010854520305865.

7 S. Hsu, S. Rommel, P. Eversfield, K. Muller, E. Klemm, W. Thiel, et al., A rechargeable hydrogen battery based on Ru catalysis, Angew. Chem., Int. Ed., 2014, 53(27), 7074–7078, DOI: 10.1002/anie.201310972.

8 T. Liu, Z. Liu, G. Kim, J. T. Frith, N. Garcia-Araez and C. P. Grey, Understanding LiOH chemistry in a ruthenium-catalyzed Li–O_2 battery, Angew. Chem., Int. Ed., 2017, 56(50), 16057–16062, DOI: 10.1002/anie.201709886.

9 E. Antonarakis and A. Emadi, Ruthenium-based chemotherapeutics: are they ready for prime time?, Cancer Chemother. Pharmacol., 2010, 66, 1–9.

10 C. S. Allardyce and P. J. Dyson, Ruthenium in medicine: current clinical uses and future prospects, Platin. Met. Rev., 2001, 45, 62.

11 M. Kolbe, P. Hönicke, M. Müller and B. Beckhoff, L-subshell fluorescence yields and Coster–Kronig transition probabilities with a reliable uncertainty budget for selected high- and medium-Z elements, Phys. Rev. A, 2012, 86, 042512.

12 M. Kolbe and P. Hönicke, Reliable determination of fundamental parameters of Zr and Ti for a reliable quantitative X-ray fluorescence analysis, X-Ray Spectrom., 2015, 44(4), 217–220.

13 Y. Kayser, P. Hönicke, M. Wansleben, A. Wählisch and B. Beckhoff, Experimental determination of the gadolinium L subshells fluorescence yields and Coster–Kronig transition probabilities, X-Ray Spectrom., 2022, (1), DOI: 10.1002/xrs.3313.

14 P. Hönicke, R. Unterumsberger, N. Wauschkuhn, M. Krämer, B. Beckhoff, P. Indelicato, et al., Experimental and theoretical approaches for determining the K-shell fluorescence yield of carbon, Radiat. Phys. Chem., 2022, 110501.

15 N. Wauschkuhn, K. Frenzel, B. Beckhoff and P. Hönicke, Experimental determination of tantalum L-shell fluorescence yields and Coster–Kronig transition probabilities, J. Anal. At. Spectrom., 2023, 38, 197–203, DOI: 10.1039/D2JA00325B.

16 M. Krumrey, Design of a four-crystal monochromator beamline for radiometry at BESSY II, J. Synchrotron Radiat., 1998, 5(1), 6–9.

17 M. Kolbe, B. Beckhoff, M. Krumrey and G. Ulm, Thickness determination for Cu and Ni nanolayers: comparison of reference-free fundamental-parameter based X-ray fluorescence analysis and X-ray reflectometry, Spectrochim. Acta B, 2005, 60, 505–510.

18 F. Scholze and M. Procop, Modelling the response function of energy dispersive X-ray spectrometers with silicon detectors, X-Ray Spectrom., 2009, 38(4), 312–321.

19 P. Hönicke, M. Kolbe, M. Müller, M. Mantler, M. Krämer and B. Beckhoff, Experimental verification of the individual energy dependencies of the partial L-shell photoionization cross sections of Pd and Mo, Phys. Rev. Lett., 2014, 113(16), 163001.

20 Y. Ménesguen, M. C. Lépy, J. M. Sampaio, J. P. Marques, F. Parente, M. Guerra, et al., A combined experimental and theoretical approach to determine X-ray atomic fundamental quantities of Tin, X-Ray Spectrom., 2018, 47(5), 341–351.

21 J. Sherman, The theoretical derivation of fluorescent X-ray intensities from mixtures, Spectrochim. Acta, 1955, 7, 283–306.

22 B. Beckhoff, Reference-free X-ray spectrometry based on metrology using synchrotron radiation, J. Anal. At. Spectrom., 2008, 23, 845–853.

23 H. Ebel, R. Svagera, M. F. Ebel, A. Shaltout and J. H. Hubbell, Numerical description of photoelectric absorption coefficients for fundamental parameter programs, X-Ray Spectrom., 2003, 32, 442–451.

24 R. Unterumsberger, P. Hönicke, J. Colaux, C. Jeynes, M. Wansleben, M. Müller, et al., Accurate experimental

This journal is © The Royal Society of Chemistry 2023

J. Anal. At. Spectrom., 2023, 38, 1301–1306 | 1305

determination of gallium K- and L_3-shell XRF fundamental parameters, *J. Anal. At. Spectrom.*, 2018, **33**(6), 1003–1013.

25 T. Schoonjans, A. Brunetti, B. Golosio, M. S. del Rio, V. A. Solé, C. Ferrero, *et al.*, The xraylib library for X-ray–matter interactions. Recent developments, *Spectrochim. Acta B*, 2011, **66**, 776–784.

26 M. O. Krause, Atomic radiative and radiationless yields for K and L shells, *J. Phys. Chem. Ref. Data*, 1979, **8**(2), 307–327.

27 S. Puri, D. Mehta, B. Chand, N. Singh and P. N. Trehan, L shell fluorescence yields and Coster–Kronig transition probabilities for the elements with $25 \leq Z \leq 96$, *X-Ray Spectrom.*, 1993, **22**(5), 358–361.

28 E. McGuire, Atomic L-shell Coster–Kronig, Auger, and radiative rates and fluorescence yields for Na-Th, *Phys. Rev. A*, 1971, **3**(2), 587.

29 S. T. Perkins, D. E. Cullen, M. H. Chen, J. Rathkopf, J. Scofield, and J. H. Hubbell, Tables and graphs of atomic subshell and relaxation data derived from the LLNL evaluated atomic data library (EADL), $Z = 1$–100, UCRL-50400-Vol-30, 1991.

30 J. Xu and E. Rosato, Relative intensities of diagram and satellite L-X-rays for elements $Z = 37$–56, *J. Phys.*, 1987, **48**(C-9), 661–664.

31 P. Hönicke, M. Kolbe, M. Krumrey, R. Unterumsberger and B. Beckhoff, Experimental determination of the oxygen K-shell fluorescence yield using thin SiO_2 and Al_2O_3 foils, *Spectrochim. Acta B*, 2016, **124**, 94–98.

1306 | *J. Anal. At. Spectrom.*, 2023, **38**, 1301–1306

This journal is © The Royal Society of Chemistry 2023